

Probing the Fibrate Binding Specificity of Rat Liver Fatty Acid Binding Protein

Sara Chuang,[†] Tony Velkov,[†] James Horne,[†] Jerome Wielens,[†] David K. Chalmers,[†] Christopher J. H. Porter,^{*,‡} and Martin J. Scanlon^{*,†}

[†]*Medicinal Chemistry and Drug Action and [‡]Drug Delivery Disposition and Dynamics, Monash Institute of Pharmaceutical Sciences, Monash University (Parkville Campus), 381 Royal Parade, Parkville 3052 Victoria Australia*

Received October 24, 2008

Liver-fatty acid binding protein (L-FABP) is found in high levels in enterocytes and is involved in cytosolic solubilization of fatty acids. In addition, L-FABP has been shown to bind endogenous and exogenous lipophilic compounds, suggesting that it may also play a role in modulating their absorption and disposition within enterocytes. Previously, we have described binding of L-FABP to a range of drugs, including a series of fibrates. In the present study, we have generated structural models of L-FABP–fibrate complexes and undertaken thermodynamic analysis of the binding of fibrates containing either a carboxylic acid or ester functionality. Analysis of the current data reveals that both the location and the energetics of binding are different for fibrates that contain a carboxylate compared to those that do not. As such, the data presented in this study suggest potential mechanisms that underpin molecular recognition and dictate specificity in the interaction between fibrates and L-FABP.

Introduction

Liver fatty acid binding protein (L-FABP^a) is a member of a family of phylogenetically related low molecular weight proteins known as intracellular lipid binding proteins (iLBP). The iLBP family comprises of several classes, including sterol carrier proteins, retinol binding proteins, and cytosolic fatty acid binding proteins (FABPs).^{1,2} Although various functions have been proposed for these proteins, it is widely accepted that iLBPs enhance the effective aqueous solubility of lipophilic molecules and thereby facilitate their intracellular transport.^{3,4} Across the iLBP family, however, there are differences in ligand specificity, binding affinity, and orientation of the ligand within the binding cavity. These differences in ligand binding have been utilized to classify iLBPs into various subgroups.^{1,2,4}

FABPs are generally the most abundant proteins in the cells where they are expressed^{3,5} and they exhibit tissue-specific distribution.^{6,7} There are nine different human FABP proteins, namely: liver (L), intestinal (I), muscle and heart (H), adipocyte (A), epidermal (E), ileal (II), brain (B), myelin (M), and testis (T).^{3,5} Although the nomenclature refers to the tissue in which the FABP was first identified, FABP subtypes may be expressed in more than one tissue. For example, in addition to expression in the liver, L-FABP is expressed at high levels in enterocytes.^{3,5} FABPs possess similar tertiary structures and are composed of 10 antiparallel β -strands, which form a barrel with a clamshell-like structure. The barrel

is capped by a pair of α -helices, which enclose a cavity that has been shown to be the FABPs lipid-binding site.^{1–5} A mechanism for ligand binding, termed the “portal hypothesis”,⁸ has been proposed where the natural ligand (FA) enters the protein through a dynamic area, consisting of the second α -helix and the turns between β -strands β C– β D (Tyr⁵⁴–Gly⁵⁵ in L-FABP) and β E– β F (Glu⁷²–Thr⁷³ in L-FABP), before binding inside the cavity.⁸ The dynamic area through which entry occurs is described as the “portal region”.⁸ Although the sequence conservation between FABPs is not high in the portal region (Supporting Information Table 1), it has been shown that mutating the bulky portal residues of murine A-FABP to glycine has a dramatic effect on the rate of binding and dissociation without altering ligand affinity or selectivity.⁸

Overall, human FABPs display a 38–70% sequence identity,⁹ while rat FABPs display 15–64% sequence identity (Supporting Information Table 1). The need for proteins with a high degree of similarity, yet distinct differences in tissue distribution and ligand binding selectivity, suggests the potentially specialized function of these individual proteins.⁴ Furthermore, comparison of the FABPs from different species indicates that significant sequence similarity exists between the same FABPs of different mammalian species.⁹ For instance, rat and human L-FABP display sequence identity of 82% with many amino acid differences being conservative substitutions¹⁰ (Supporting Information Table 1). Consequently, studies of rat L-FABP (rL-FABP) can potentially provide information relating to the function of L-FABP in humans.

Although structurally similar to other members of the FABP family, L-FABP is distinct because of its larger binding cavity, which has a solvent accessible surface area of 610 Å².^{11,12} In comparison, other members of the FABP family have cavities ranging from 334–510 Å².¹¹ X-ray crystallography studies of rL-FABP in complex with oleic acid¹² demonstrated that

*To whom correspondence should be addressed. Phone +61 3 99039540 (M.J.S.) or +61 3 99039649 (C.J.P.). Fax: +61 3 9903 9582. E-mail: Martin.Scanlon@pharm.monash.edu.au (M.J.S.) or Chris.Porter@pharm.monash.edu.au (C.J.P.).

^aAbbreviations: CSP, chemical shift perturbations; L-FABP, liver fatty acid binding protein; FA, long chain fatty acid; DMSO, dimethyl-sulfoxide; HSQC, ¹H–¹⁵N-heteronuclear single quantum coherence; iLBP, intracellular lipid binding proteins; PPAR, peroxisome proliferator-activated receptor; vdW, van der Waals.

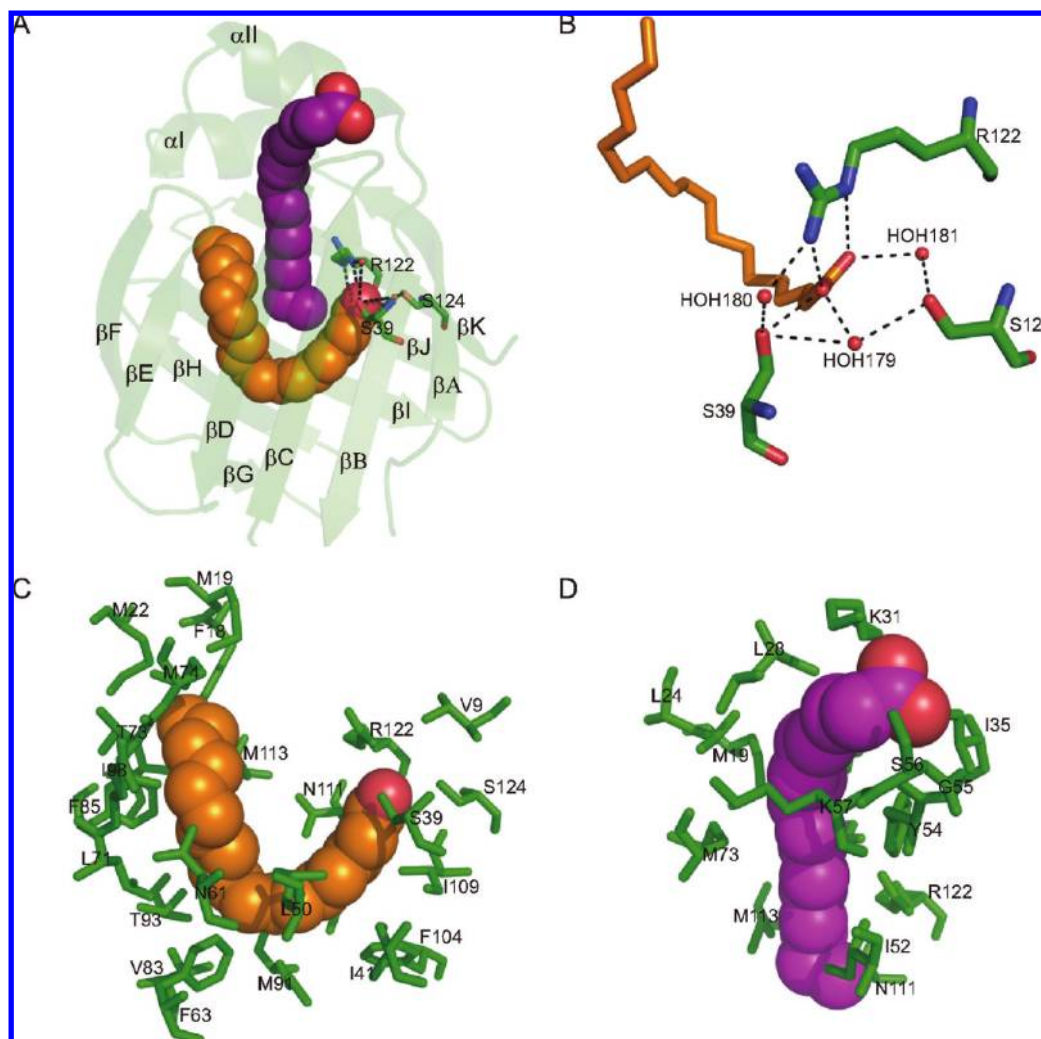


Figure 1. Crystal structure of rat L-FABP in complex with two oleates (1LFO) (A) Ribbon representation of L-FABP with two bound oleates shown in sphere representation. Elements of secondary structure are labeled from N–C terminus. Residues involved in forming the hydrogen bonding network with the carboxylate headgroup of the oleate at high affinity (internal) site are shown in stick representation. Structured water molecules also involved in hydrogen binding are shown as red spheres. Oleates are shown in CPK representation. The oleate bound at the high affinity site is colored orange and that at the low affinity site is colored purple. (B) Hydrogen bonding network at the high affinity binding site. rL-FABP residues involved in H-bonds are annotated and shown in green stick representation. Structured water molecules are shown as red spheres and annotated 179–181. (C) Oleate bound at the high affinity binding site and (D) oleate bound at the low affinity binding site of L-FABP. Residues within 4.5 Å are shown as in green stick representation and labeled. This illustration was prepared with the use of PyMol v0.99.

rL-FABP binds oleic acid at a stoichiometric ratio of 1:2, whereas other iLBP typically bind with a stoichiometry of 1:1. The first FA molecule, which binds at a higher affinity ($\sim 9\text{--}200\text{ nM}^{13\text{--}15}$), is fully enclosed within the β -barrel structure of the protein in a bent conformation where the carboxylate group forms a hydrogen bonding network within the binding pocket (Figure 1). Hydrogen bonds are formed between the side chain of Arg¹²², the side chain of Ser³⁹, and a single oxygen of the fatty acid molecule. Ser¹²⁴, Arg¹²², and oleic acid form hydrogen bonds to three structured water molecules such that Ser¹²⁴ interacts with the fatty acid molecule indirectly (Figure 1B). The second FA, which binds with lower affinity ($0.9\text{--}2.9\text{ }\mu\text{M}^{13\text{--}15}$), binds “tail first” with the carboxylate group protruding from the protein (Figure 1D).¹² The second FA consequently binds mainly via hydrophobic forces. While L-FABP is known to bind FA with high affinity, it has also been found to bind a range of other compounds, including bile salts, bilirubin, lysophospholipids, cyclopentenone, and other hydrophobic compounds, including a range of lipophilic drugs with reported affinities ranging

from high nM to low mM.^{3,13,16} The ability to bind to a diverse range of lipophilic molecules was initially thought to be dictated by the presence of the second “lipophilic” binding pocket, where lipophilic molecules could bind in a relatively nonspecific manner within the low affinity FA binding site.^{3,13,16} However, we have recently shown that rL-FABP has the ability to bind drug molecules at both FA binding sites and that a carboxylate is not required for high-affinity binding at the internal site.¹³

In the present study, we have examined the binding interactions between rL-FABP and a series of fibrates. Clinically, the fibrates are used to lower serum lipid levels (hypolipidemic agents) and appear to act via interaction with the nuclear receptor peroxisome proliferator activated receptor α (PPAR α).¹⁶ Previous studies have suggested that fibrate binding to FABP may provide for both cytoplasmic solubilization and a mechanism by which poorly water-soluble drugs are shuttled to their target receptor (PPAR).¹⁷

Fibrate binding to rL-FABP was assessed initially by employing nuclear magnetic resonance (NMR) chemical shift

perturbation (CSP) experiments. These data were utilized to analyze modes of binding at each site of rL-FABP as assessed by molecular modeling studies. Thermodynamic parameters for the two most structurally similar fibrates, fenofibric acid and fenofibrate, as well as a second ester clofibrate, were derived from the temperature dependence of the binding affinities determined by equilibrium fluorescence measurements. These data were used to dissect the driving forces for binding interactions at the two sites and for ligands that contain or lack the terminal carboxylate that is present in the natural ligand (FA). The investigation has provided new insights into how rL-FABP accommodates two fibrate molecules and, in particular, proposes a mechanism by which compounds lacking a carboxylate may bind with high affinity to rL-FABP.

Results

Choice of Test Compounds. The compounds employed in this study were a series of fibrates which have previously been shown to bind to rL-FABP.¹³ The fibrates contain a common isopropyl (or isohexyl in the case of gemfibrozil) phenyl ether structural element and either a carboxylate terminus (fenofibric acid, gemfibrozil, bezafibrate, and ciprofibrate) or an ester terminus (fenofibrate and clofibrate). While structurally similar, the series of fibrates examined have different physicochemical properties. Calculated LogP (octanol:water partition coefficient) values for the molecules ranged between 2.9–4.8. However, calculated LogD (apparent octanol:water distribution coefficient) at the experimental pH showed a broader range between 0.69–4.8 (Table 1). This is reflected in significant differences in the calculated aqueous solubility of the fibrates tested (Table 1). Despite the general similarity of the test compounds, they have binding affinities for rL-FABP that span more than an order of magnitude (Table 1). Previous data have shown that compounds with greater lipophilicity generally have higher affinity for L-FABP,¹⁵ but this is not the case for this series of fibrates. As such, their binding to rL-FABP appears to be driven by specific interactions within the binding cavity.

Chemical Shift Perturbations and Analysis. Fibrate binding was examined via CSP studies by measuring changes in the ¹³C_α and ¹³C_β chemical shifts of rL-FABP in CBCA(CO)NH experiments upon saturation with drug (Supporting Information Table 2). CSPs for amide protons and nitrogens are usually readily measured from ¹H–¹⁵N HSQC spectra, but in the current studies, titration of rL-FABP with several of the fibrates resulted in significant line broadening although the spectra of both the apoprotein and the fully saturated protein were of good quality for each of the test compounds (Supporting Information Figure 1). As a consequence, it was not possible to track the perturbations by recording HSQC spectra at different rL-FABP:drug ratios as we have reported previously.^{13,18} Rather, assignments were generated for apo- and drug-saturated rL-FABP by recording standard triple resonance NMR spectra for each fibrate complex. This approach enabled the generation of sequence-specific assignments of H, N C_α and C_β resonances for each complex. CSPs for amide protons and nitrogens can often result due to indirect structural perturbations, which can complicate interpretation of the data to identify binding site location. In contrast, changes in C_α and C_β shifts have been shown to be more specific¹⁹ and thus these were utilized to provide a greater degree of discrimination of binding

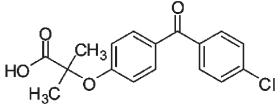
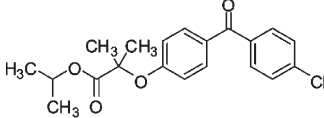
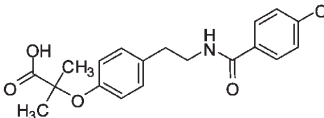
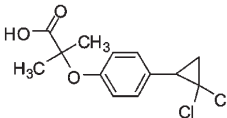
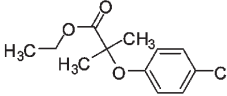
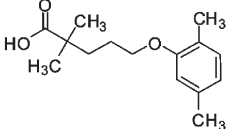
interactions. Although indirect structural perturbations are also observed for ¹³C resonances, presumably as a result of the conformational changes that occur upon ligand binding,^{12,20} we have previously demonstrated that upon titration of rat I-FABP with palmitic acid, the largest perturbations are observed for residues that are adjacent to the ligand binding site identified in the structure of the complex.¹⁹

Initial studies compared the chemical shift perturbations of fenofibrate and fenofibric acid. These were the most structurally similar compounds examined, differing only in the presence of an isopropyl ester group in fenofibrate, compared to a terminal carboxylate in fenofibric acid. The chemical shift perturbations observed upon formation of the fibrate:rL-FABP complex are mapped onto the crystal structure of holo-rL-FABP (1LFO) (Figure 2). It is evident that different subsets of peaks were perturbed upon binding of fenofibric acid compared to fenofibrate. There were 12 residues whose chemical shifts were perturbed by more than one standard deviation above the mean upon titration of rL-FABP with 3 mol equiv of fenofibric acid. The perturbed residues are mapped onto the structure of rL-FABP (1LFO) (Figure 2C). The residues whose ¹³C_α and ¹³C_β resonances experienced the greatest CSPs upon binding include Ser¹²⁴, Thr¹¹⁰, Leu⁵⁰, and Val³⁸. These residues are all adjacent to the triad of residues Ser¹²⁴, Ser³⁹, and Arg¹²², which form the hydrogen bonding network for the carboxylate headgroup of FA¹². These perturbations suggest that a similar ionic interaction may be present in the complex with fenofibric acid. Other perturbed residues include Glu⁶², Glu⁷², and Ile⁹⁸, which are also in the vicinity of the high affinity site in the complex with oleic acid and have been shown previously to interact with the hydrophobic tail of the fatty acid¹². Met²², Lys³⁶, Thr⁷³, Thr⁷⁵, and Tyr¹²⁰ were also significantly perturbed. These residues are located either within the helical element (Met²²), the portal region (Thr⁷³, Thr⁷⁵), or close to the region where the helices connect to the barrel (Lys³⁶ and Tyr¹²⁰) and are closer to the low affinity FA binding site in the structure of rL-FABP.

Upon addition of 3 mol equiv of fenofibrate to rL-FABP, there were also 12 residues that exhibited CSPs greater than one standard deviation above the mean change. However, the pattern of perturbations was significantly different (Figure 2B). Thus, in the vicinity of the high-affinity site, although a number of polar residues were perturbed including Lys⁴⁹, Thr⁵¹, Asn⁶¹, and Ser¹⁰⁰ residues adjacent to the carboxylate binding site were not as significantly perturbed as was the case with fenofibric acid. The hydrophobic residues, Tyr⁷, Met⁹¹, and Val⁹², which are located toward the base of the β-barrel, were also significantly perturbed upon binding of fenofibrate, as were residues Leu⁵⁰ and Val¹⁰¹, which are located at the center of the β-sheets. Of the 12 residues that experienced the largest CSPs, only three were in the vicinity of the low affinity binding site. On the second α-helix Met¹⁹ and Met²² were perturbed, while Thr⁵³, which is adjacent to the portal region, was also perturbed.

Comparing the CSPs upon addition of fenofibric acid and fenofibrate, distinct differences were observed. For fenofibric acid, large C_α and C_β CSPs were observed for residues that span the central portion of the β-sheets. Conversely, the cluster of perturbed residues observed upon fenofibrate binding were buried deeper within the β-barrel. Furthermore, residues previously associated with carboxylate binding at the high affinity site were perturbed by fenofibric acid but not by fenofibrate. These differences in

Table 1. Physicochemical Properties of Ligands^a

Ligand	MW	LogP [†]	LogD pH5.5 [‡]	PSA [^]	Ki ₁ (μM) [*]	Ki ₂ (μM) [*]	cSol [†] (g/L)
Fenofibric Acid 	318.75	3.9	1.5	64	0.33	28	4.3
Fenofibrate 	360.83	4.8	4.8	53	0.024	0.41	0.020
Bezafibrate 	361.82	3.5	1.3	76	44	N/A	2.5
Ciprofibrate 	289.15	2.9	0.69	47	0.58	110	29
Clofibrate 	242.70	3.3	3.3	36	6.9	N/A	0.050
Gemfibrozil 	250.33	4.4	3.6	47	1.9	180	0.17

^a*Obtained from ref 13. [†]Calculated using ACD software v6.00 (ACD/Laboratories, Toronto, Canada). [^]Calculated using ChemBioDraw Ultra v.11 (CambridgeSoft, USA).

perturbations suggest that binding of fenofibrate and fenofibric acid is mediated via different specific interactions. In the low affinity binding site, a greater number of polar residues were perturbed upon addition of fenofibric acid compared to fenofibrate.

The differences in binding observed at the high affinity site most likely reflect the different chemical moieties

(i.e., carboxylate or ester) present in the two molecules. To assess more broadly the impact on binding of the presence of a carboxylate or ester functionality within the molecule, chemical shift perturbation maps were obtained for bezafibrate, ciprofibrate, and gemfibrozil, which possess a terminal carboxylate group, and clofibrate, which is an ethyl ester. The binding profiles of the carboxylate fibrates

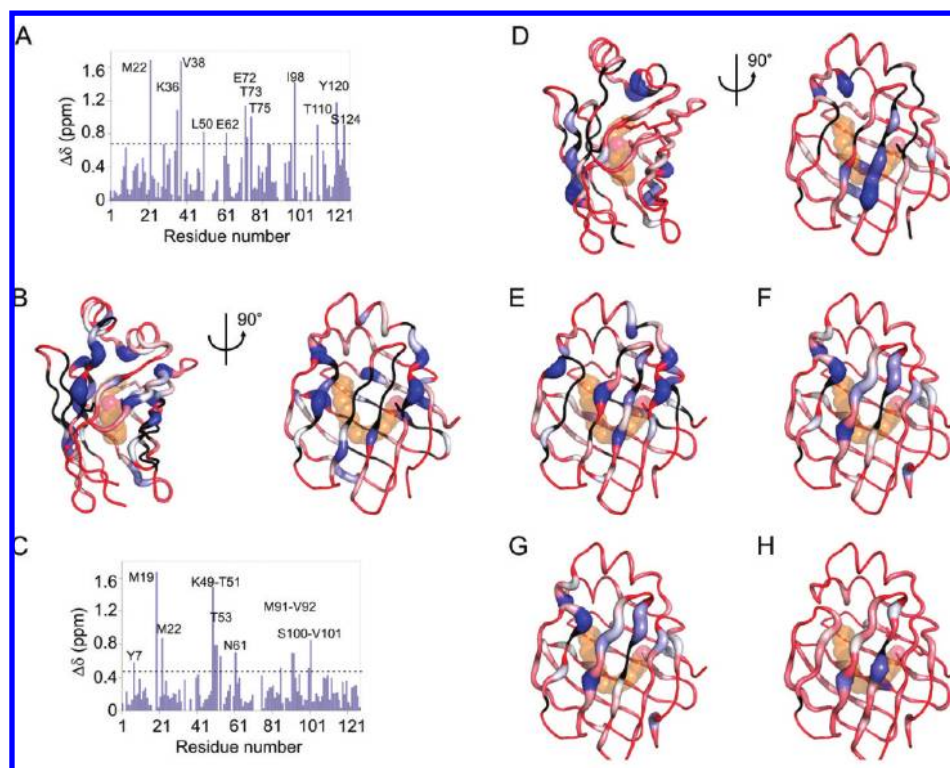


Figure 2. Measured $^{13}\text{C}_\alpha$ and $^{13}\text{C}_\beta$ chemical shift perturbations upon addition of fenofibric acid (A) and fenofibrate (C). Residues with CSPs greater than one standard deviation above the mean are labeled. (C–H) rL-FABP is depicted as a variable width ribbon, where the width of the ribbon is dictated by the extent of the CSP observed upon addition of (B) fenofibric acid or (D) fenofibrate. The two views are rotated by 90° about the y axis. The ribbon is colored on a color ramp from red to blue, where red represents no CSP and blue represents the largest CSP observed for the data set. Residues for which no assignments could be made in the NMR spectra are colored black. The oleate molecule bound at the high affinity site of rL-FABP is shown in CPK. Similar ribbon diagrams are shown depicting CSPs observed upon addition of (E) bezafibrate, (F) ciprofibrate, (G) gemfibrozil, and (H) clofibrate. For each compound that contains a carboxylic acid (C, E, F, G), significant perturbations are observed around the location of the carboxylate in the crystal structure of the complex with oleate. In contrast, the esters (D, H) do not significantly perturb the residues around the carboxylate in the complex with oleate.

(bezafibrate, ciprofibrate, and gemfibrozil in Figure 2) showed a similar general trend to fenofibric acid where residues perturbed spanned the β -barrel and the polar regions. The three residues that form the hydrogen bonding network to the carboxylate of FA in the high affinity site (Ser³⁹, Arg¹²², and Ser¹²⁴) consistently exhibited significant perturbation or peak broadening beyond the limit of detection for all the carboxylate-containing fibrates. The similarity observed in the patterns of perturbations for these fibrates is consistent with the formation of a similar network of interactions in the binding cavity, as seen previously for oleic acid in the crystal structure. Conversely, a similar cluster of residues were perturbed in both fenofibrate and clofibrate (Figure 2), which were distinct from those perturbed by the carboxylates, namely Met⁹¹, Ser¹⁰⁰, Leu⁵⁰, Thr⁵¹, and Asn⁶¹ located centrally in the β -barrel. In addition, the esters caused far less perturbation of Ser³⁹, Arg¹²², and Ser¹²⁴. This suggests that the esters may be stabilized via similar interactions to one another but via a different mechanism to that observed with carboxylate-containing compounds. Binding at the low affinity binding site showed significant variation in the pattern of perturbed residues for each of the different fibrates. This may reflect the greater structural variation that is present within the “lipophilic” portion of the fibrate structures and is consistent with this lipophilic portion of fibrate molecules binding in a similar manner to FA in the low affinity binding site of rL-FABP.

Docking Studies. To characterize the potentially different modes of binding, docking studies were carried out in which each of the fibrates was docked into the FA-binding sites of L-FABP. Such docking calculations generate numerous different binding orientations or “poses”, which can be grouped into “clusters” of similar poses. Clusters observed for each of the fibrates were compared with perturbations measured in the NMR data in an attempt to identify the closest matching binding orientation. The following scoring system was used to determine the cluster that best matched the perturbation data. Residues were given an arbitrary score of 1 if they were within the clusters and also displayed significant CSPs in the NMR data, 0.5 if a CSP was observed for a residue adjacent to one of the residues in the docking cluster, and 0 for residues in the docking clusters that were not observed or not assigned in the spectra of the complex due to peak broadening. Residues within the docking clusters, which were assigned but not perturbed, were given a score of -1 . The highest scoring docking solutions for each of the fibrates are shown in Figures 3 and 4. The interactions formed between each of the drugs and rL-FABP in the highest scoring pose are summarized schematically in Figure 5.

A single docking cluster was found for fenofibric acid in the high affinity site (Figure 3A–C). In the docking solution, the carboxylate of fenofibric acid formed hydrogen bonds with Arg¹²² and Ser³⁹. Hydrophobic interactions between

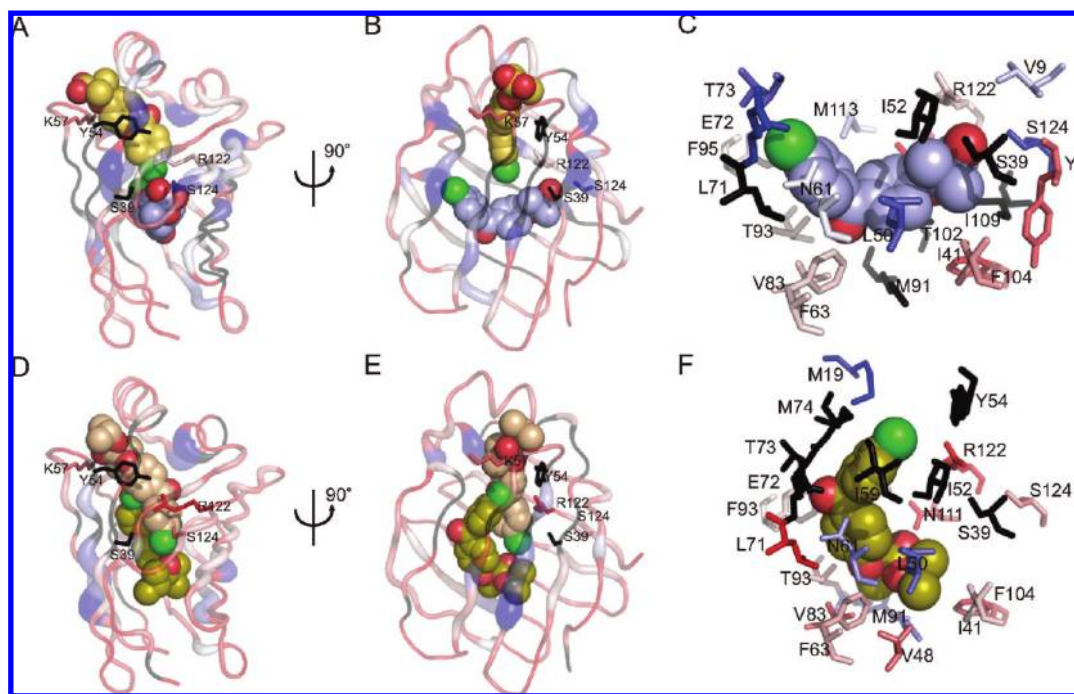


Figure 3. Docking solutions for (A–C) fenofibric acid and (D–F) fenofibrate binding at the high affinity site of rL-FABP. The protein is depicted as a variable width ribbon and colored as in Figure 2. Residues involved in the H-bond network in the complex with oleate (S₃₉, R₁₂₂, S₁₂₄) are shown in stick representation and labeled as are the portal residues (Y₅₄, K₅₇) that play a role in oleate binding at the low affinity site of rL-FABP. (A–B) The optimal docking solution for fenofibric acid at the high affinity site is shown in blue sphere representation and at the low affinity site in gold sphere representation. (C) Residues within 3 Å of the docked structure of fenofibric acid are shown in stick representation and colored by the extent of observed CSP as described. Several of the most significantly perturbed residues (blue) or residues for which no assignments could be obtained cluster at the docked location of fenofibric acid. (D–E) Optimal docking solutions for fenofibrate at the high (yellow) and low (coral) affinity sites, respectively. (F) Residues within 3 Å of the docked structure of fenofibrate are shown in stick representation and colored by the extent of observed CSP as described.

fenofibric acid and rL-FABP involved residues Ile¹⁰⁹, Met¹¹³, Phe⁹⁵, Leu⁷¹, Ile⁵², and Leu⁵⁰. Figure 3C demonstrates that several of the residues whose chemical shifts are most significantly perturbed upon addition of fenofibric acid or whose peaks exhibit significant broadening in the NMR spectra either interact directly with the ligand in the docking cluster or are adjacent to residues that are making interactions with the ligand. There is therefore a good correlation between the recorded chemical shift perturbations and the orientation of binding identified by docking.

Fenofibrate, on the other hand, was found to have two docking clusters, one comprised of four docking poses and the other comprised of one. The first cluster (Figure 3D–F) displayed the better correlation with NMR data. A hydrogen bond was present between Thr¹⁰² and the carbonyl oxygen of the ester. Other contacts along the length of the fenofibrate molecule (Met⁹¹, Val⁸³, Val⁴⁸, Leu⁵⁰, Ile⁵², Ile⁵⁹, Met⁷⁴, Phe⁹⁵, and Leu⁷¹) were hydrophobic in nature. As observed with fenofibric acid, many of the residues that made interactions with the ligand in the docked structure were either those whose C_α and C_β resonances were most significantly perturbed upon addition of fenofibrate, exhibited peak broadening, or were adjacent to such residues (Figure 3F). To assess the role of the isopropyl group of fenofibrate on the binding orientations observed in the docking, a second docking experiment was performed with the methyl ester of fenofibric acid. For the methyl ester, the clusters with the highest docking scores matched very closely the orientations observed in the docking clusters of fenofibrate (Supporting Information Figure 2). The similar mode of binding observed for the methyl and isopropyl esters suggests that the

nature of the small aliphatic ester group is not a dominating factor in dictating the binding orientation.

Comparing the docking solutions and the perturbations of fenofibric acid and fenofibrate, it can be seen that the binding sites of the two molecules are significantly different as depicted in Figure 3. The carboxylate terminus of fenofibric acid is bound in a similar manner to the carboxylate group of oleic acid in the crystal structure (Figure 1B), with a hydrogen bonding network involving Arg¹²² and Ser³⁹. The presence of a strong interaction between the carboxylate and Arg¹²² may contribute to the observation of only a single docking pose for fenofibrate at this site. The remainder of the fenofibric acid forms a number of hydrophobic interactions and occupies a similar position to the midregion of the methylene tail of oleic acid in the crystal structure. In contrast, the complex with fenofibrate has a hydrogen bond between Thr¹⁰² and the carbonyl oxygen of the ester group, while the remainder of the fenofibrate forms hydrophobic interactions within the cavity. Fenofibrate is not interacting with Arg¹²² and Ser³⁹ as seen with fenofibric acid and oleic acid, although the hydrophobic contacts are consistent with the location of the terminal portion of the methylene tail of oleic acid (Figure 1C).

For the remaining carboxylate-containing fibrates, bezafibrate and ciprofibrate were both found to have four docking clusters, while gemfibrozil had two. The highest scoring clusters in each case showed the carboxylate forming a hydrogen bond with at least one of Arg¹²², Ser¹²⁴, and Ser³⁹ (Figures 4 and 5). The use of the CSPs to refine docking clusters suggest that the binding of all four carboxylates in the high affinity site is anchored via a similar hydrogen

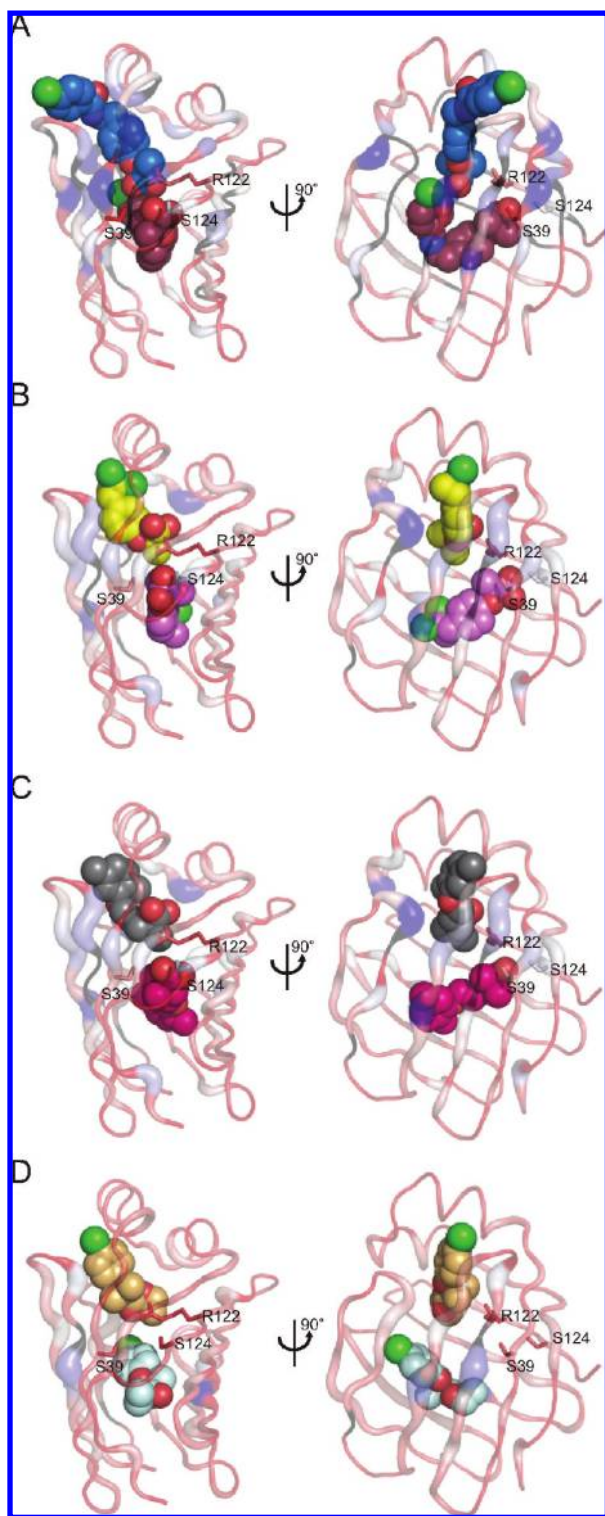


Figure 4. Docking solutions for (A) bezafibrate, (B) ciprofibrate, (C) gemfibrozil, and (D) clofibrate. Optimal docking solutions are depicted for each drug at the high and low affinity sites, respectively. Residues involved in the H-bond network in the complex with oleate (S₃₉, R₁₂₂, S₁₂₄) are shown in stick representation. (A–C) In the optimal docking solution for each of the fibrates containing a carboxylate, the carboxylate group is docked in a position where similar interactions to those observed with oleate in the crystal structure of the complex could be formed. Significant CSPs are observed in each case for residues involved in or adjacent to the H-bond network with oleate. In contrast, with clofibrate (D), the ester is docked at a different location and smaller CSPs are observed for the residues involved in the H-bond network. The protein is depicted as a variable width ribbon and colored as in Figure 2.

bonding network to that observed in the oleic acid crystal structure. Examination of clofibrate docking revealed only one docked cluster (Figure 4D), which also showed hydrogen bonding from the carbonyl oxygen of the ester to Thr¹⁰², the chemical shifts of which were significantly perturbed upon addition of clofibrate. Docking solutions of the ester compounds, fenofibrate, and clofibrate in the high affinity binding site showed van der Waals (vdW) contacts to Leu⁵⁰, Leu⁷¹, and Met⁹¹, which either exhibited significantly perturbed C_α and C_β resonances or were adjacent to residues with significantly perturbed resonances.

The docking clusters that were observed for fenofibric acid in the low affinity binding site, differed in buried depth within the binding cavity. The higher scoring docking cluster was buried deeper within the barrel cavity and formed a polar interaction with Leu²⁸. Among the residues that participated in hydrophobic interactions in the docking cluster, many displayed significant CSPs (Tyr¹²⁰), exhibited peak broadening (Gly³², Ile⁵², Lys⁵⁷, Met⁷⁴) or were adjacent to residues which did (Arg¹²²) (Figure 3). The CSP-refined docking solutions are consistent with fenofibric acid occupying a similar orientation to oleic acid in the low affinity binding site of the crystal structure (1LFO).

Docking of fenofibrate to the low affinity binding site generated seven docking clusters. The clusters displayed a mix of orientations (Supporting Information Figure 3), with the ester terminus located either buried within the barrel or protruding from the β-barrel. For the highest scoring cluster, the ester terminus was protruding from the β-barrel (Figure 3). No hydrogen bonding was identified in this cluster. The interactions observed in the docked complex were entirely hydrophobic (Figure 5) and located at either the α-helical region (Met¹⁹, Leu²⁸, Lys³¹, Gly³²) or at the portal region (Tyr⁵⁴, Lys⁵⁷, Met⁷⁴). Several of these residues displayed significantly perturbed C_α and C_β resonances in the NMR spectra (Met¹⁹) were adjacent to such residues (Tyr⁵⁴) or exhibited peak broadening (Lys³¹, Gly³², and Met⁷⁴) (Figure 3). Analysis of the remaining six docking clusters resulted in a similar number of correlations between the docking clusters and perturbed residues, differing primarily in the depth to which the molecule was buried within the β-barrel. However, residues that both exhibited significant CSPs and matched the docking clusters were generally located at the portal region, indicating that fenofibrate was likely to reside within the area specified by the docking clusters.

At the low affinity site of rL-FABP, fenofibric acid and fenofibrate were observed to interact with residues that formed the binding site for oleic acid in both the crystal structure¹² and a recent NMR structure.²⁰ The docking solutions for fenofibrate and fenofibric acid at the low affinity site consisted of similar hydrophobic contacts, however, in both cases, fewer residues displayed significant CSPs than what was observed at the high affinity site.

Analysis of the docking clusters for the remaining fibrates revealed similar binding orientations to fenofibrate and fenofibric acid, with clusters differing largely in the depth to which the molecule was buried in the β-barrel. However, for all the fibrates, Lys⁵⁷ and Tyr⁵⁴ exhibited significant perturbation or peak broadening or were adjacent to residues which did (Figures 3 and 4). These residues are located at the portal region, which suggests that all the fibrates bind in a similar locality, albeit with lower specificity than was observed at the high affinity site. Thus the CSP data provided

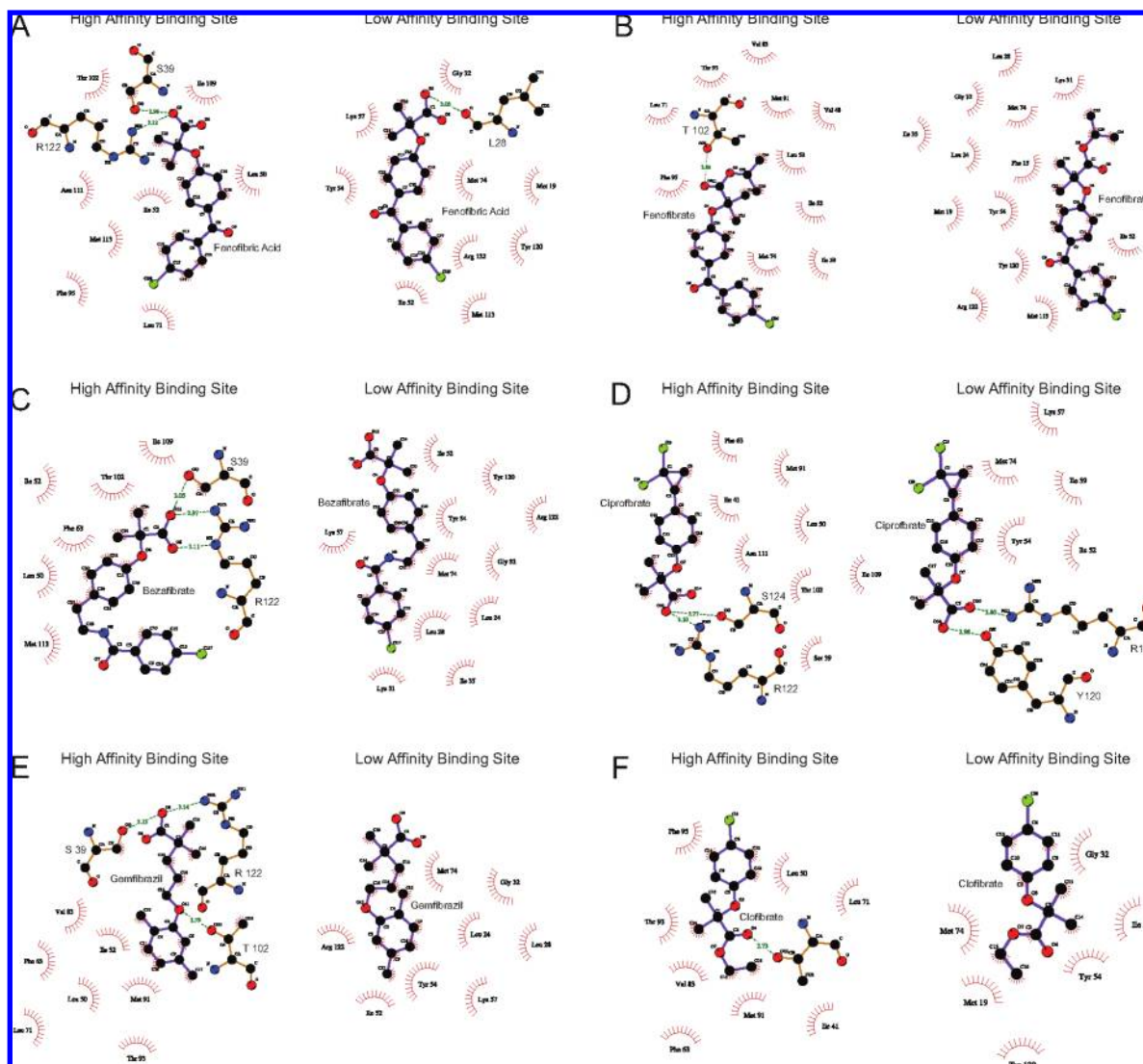


Figure 5. Ligplot representations of highest scoring docking clusters are shown for the high affinity and low affinity sites in the left and right panels, respectively. Fibrates shown are (A) fenofibric acid, (B) fenofibrate, (C) bezafibrate, (D) ciprofibrate, (E) gemfibrozil, and (F) clofibrate.

less discrimination between the different docking clusters at the low affinity site. However, the CSPs that were observed are consistent with the fibrates binding at the low affinity site in a similar location to oleic acid in the crystal structure. Neither the NMR nor the docking data exclude the possibility that there is more than one mode of binding for some or all of these compounds at the low affinity site. It is possible, therefore, that the low affinity site of L-FABP supports binding of lipophilic molecules in a relatively nonspecific manner as has been suggested previously.^{11,12} In this regard, it is perhaps noteworthy that rank order of affinity for the fibrates at the low affinity site tracks with the cLogP values for the fibrates. This is not the case for binding at the high affinity site where more specific interactions can be identified between the fibrates and rat L-FABP in the docking solutions.

Thermodynamics of Fenofibric Acid and Fenofibrate Binding to L-FABP. To determine the energetic contributions of binding to rL-FABP, the free energy (ΔG°), enthalpy (ΔH°), and entropy ($T\Delta S^\circ$) changes for the binding of fenofibric acid, fenofibrate, and clofibrate were calculated. Van't Hoff enthalpies were determined from analysis of drug binding

affinities measured at several temperatures (Figure 6, Supporting Information Table 3). The temperature dependence of the data for each compound was linear, suggesting that there were minimal changes in heat capacity over the temperature range used. The corresponding van't Hoff thermodynamic parameters are reported in Table 2.

The thermodynamic analysis revealed that fenofibric acid binding to the high affinity site was predominantly enthalpy driven with a small unfavorable entropic component, consistent with ligand binding being dominated by short-range forces such as vdW contacts, ionic interactions, and hydrogen bonds. The data were also consistent with thermodynamic parameters reported for oleic acid binding to this site as measured by the ADIFAB method²¹ and with the docking solution, which suggests that fenofibric acid binds in a similar fashion to oleic acid. In contrast, for fenofibrate, the free energy of binding at the high affinity site possessed a significantly greater entropic component than fenofibric acid and a smaller enthalpic component (Table 2; Figure 6). The less favorable enthalpy change observed upon fenofibrate binding at the high affinity site is consistent with the absence of the carboxylate functional group. In the structures of the

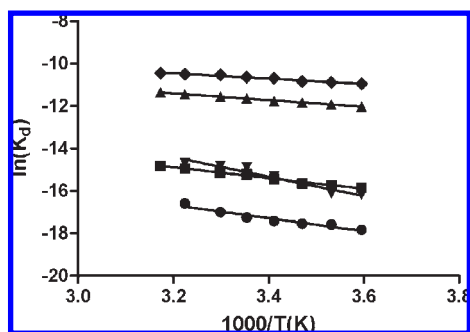


Figure 6. Thermodynamic parameters for the binding of fenofibric acid and fenofibrate to rat L-FABP. (A) Van't Hoff plots for the binding interactions for fenofibric acid at the high (\blacktriangledown) and low (\blacklozenge) affinity sites, respectively; fenofibrate at the high (\bullet) and low (\blacksquare) affinity sites, respectively; and clofibrate (\blacktriangle). The solid lines show a linear fit of the data sets, (correlation coefficients ranged from 0.95 to 0.98). Data points are the mean of three replicate experiments.

Table 2. Van't Hoff Thermodynamic Parameters for Fenofibric Acid and Fenofibrate Binding to Rat L-FABP

ligand	ΔG° (kcal/mol)	ΔH° (kcal/mol)	$T\Delta S^\circ$ (kcal/mol)
High Affinity Site			
fenofibric acid	-8.8	-9.1	-0.3
fenofibrate	-10.2	-6.2	4.0
clofibrate	-6.9	-3.2	3.7
Low Affinity Site			
fenofibric acid	-6.3	-2.6	3.7
fenofibrate	-9.0	-5.0	4.0
clofibrate	nd	nd	nd

Binding affinities were determined for temperatures between 5°C and 42°C and enthalpy values (ΔH°) were obtained from van't Hoff plots. The free energy of binding (ΔG°) values was determined from K_d values measured at 25°C. Entropy values ($T\Delta S^\circ$) was calculated from $\Delta G^\circ - \Delta H^\circ$.

oleic acid complex and in the docking model for fenofibric acid, the carboxylate forms an extensive hydrogen bonding network involving Arg¹²² and Ser³⁹ of rL-FABP, which would be expected to provide a large enthalpic contribution to binding. Conversely, the entropic contribution to binding was greater for fenofibrate than either fenofibric acid or oleic acid. The thermodynamic parameters for binding of the second ester in the study, clofibrate, appear to be consistent with this view. Clofibrate binding to rat L-FABP is characterized by a large favorable entropy term similar to that observed with fenofibrate and a smaller enthalpic term. The experimental values calculated for the binding enthalpies are consistent with the scoring functions for the docking models derived from Glide. Thus, fenofibric acid binding was accompanied by a large favorable Coulombic term in the docking—consistent with the large favorable enthalpy calculated from the fluorescence data. In contrast, the esters had favorable H-bonding terms, which are consistent with the mode of interaction observed in the docking model, and the greater affinity of fenofibrate over clofibrate is predicted by the model due to a more favorable lipophilic term and van der Waals interaction energy for fenofibrate.

At the low affinity site, fenofibric acid binding showed a marginally higher entropic component compared to the enthalpic contribution. Fenofibrate binding to both sites is driven by almost equal entropic and enthalpic components. Collectively, the thermodynamic parameters for the lower

affinity site indicate that the net free energy change for ligand binding to this site is driven by comparable entropic and enthalpic components and is consistent with the similar modes of binding observed in the docking models. No binding was detected for clofibrate at the low affinity site.

Discussion

L-FABP has previously been found to bind to a variety of hydrophobic molecules.^{3,13,16} The broad binding specificity has been suggested to arise due to the presence of a single promiscuous binding site that corresponds to the low affinity binding site for oleic acid.¹² Binding at this site was suggested to occur solely via hydrophobic interactions.^{11,12} However, more recent studies have demonstrated specific binding of structurally diverse ligands to two sites within rL-FABP under conditions where binding affinity appears not to be directly correlated with lipophilicity.^{3,13,16} These data suggest that specific interactions dictate binding. Binding interactions have been detailed previously by X-ray crystallography¹² and NMR spectroscopy²⁰ for the interaction of rL-FABP with two molecules of oleic acid, however, the structural determinants of rL-FABP binding to other ligands have not been described. In the current study, we have utilized NMR CSP studies, in conjunction with molecular docking and steady state fluorescence measurements, to probe the specificity of rL-FABP binding. We have employed a series of fibrates, which are lipid lowering agents that share a common scaffold but which differ in their affinity for L-FABP by more than an order of magnitude in order to examine more completely the determinants of rL-FABP binding to non-FA ligands.

A recently published NMR solution structure of L-FABP bound to oleic acid has suggested that at the low affinity site, Tyr⁵⁴ and Lys⁵⁷ are important contributors to ligand binding,²⁰ consistent with the previously published crystal structure.¹² The CSP and docking data describing rL-FABP binding to the range of fibrates examined here is consistent with this suggestion and indicates that the fibrates appear to bind in a similar location to FA. Previous reviews of L-FABP binding patterns have suggested that the low affinity binding site is less discriminating and typically the site of binding for ligands with bulky head groups.^{3,11,22} The current data are also consistent with this suggestion and confirm that the low affinity binding site is capable of accommodating a diverse range of ligands.

Importantly, the current studies support the finding that non-FA ligands are capable of binding in the high affinity (internal) site of rL-FABP and confirm that a terminal carboxylate is not a prerequisite for binding. FA binding to rL-FABP at the high affinity site has been shown previously to involve an ionic interaction between the FA carboxylate headgroup and the guanidinium of Arg¹²² as well as a series of hydrophobic interactions between the aliphatic tail and the binding pocket.¹² While it has been demonstrated previously that noncarboxylate containing drug molecules are capable of high affinity binding to rL-FABP,¹³ to our knowledge, the current study provides the first structural explanation for this observation.

Thus, the CSP-guided docking data suggests that the carboxylate-containing fibrates bind in a similar manner to oleic acid in complex with L-FABP. CSPs were observed that were consistent with the presence of a similar hydrogen bonding network in both cases. In contrast, the two (non-carboxylate) fibrate esters generated different CSPs in the

region around Arg¹²², suggesting that they form a differing hydrogen bonding network. However, CSPs were observed that were consistent with the “hydrophobic tail” of the two esters forming hydrophobic interactions similar to those observed with the methylene tail of oleic acid in the crystal structure of its complex with rL-FABP. These observations suggest that while ionic interactions with Arg¹²² may play a role in ligand binding to rL-FABP, this is not a prerequisite for high affinity binding at the internal site. Thermodynamic analysis revealed that binding of the carboxylate-containing fenofibric acid was predominantly driven by favorable enthalpy, whereas binding of the esters fenofibrate and clofibrate involved a larger entropic contribution, supporting the conclusion that the ionic interaction is not a prerequisite for high affinity binding. This is consistent with previous site-directed mutagenesis data, where an Arg¹²² → Gln mutation in rL-FABP resulted in only a small reduction in binding affinity for 11-(5-dimethylaminonaphthalenesulfonylamino) undecanoic acid (DAUDA) or oleic acid.²³ The mutagenesis data was subsequently extended to show that while Arg¹²² appeared to play a role in specificity and binding affinity for carboxylate-containing ligands, it was not a dominating factor in binding.²⁴

A related study with rat intestinal FABP (rI-FABP) binding to FA provides additional insights into the potential mechanism by which removal of a charge–charge interaction does not adversely affect binding affinity.²⁵ Thus, crystal structures of rI-FABP have previously shown that Arg¹⁰⁶ forms an ionic interaction in its complex with FA²⁶ and that an Arg¹⁰⁶ → Ala substitution does not reduce binding affinity. Rather, an increase of up to 28-fold in the affinity of fatty acid binding to the mutant when compared to wild-type was reported.²⁵ Examination of the thermodynamics of the binding subsequently showed that while there was a loss of enthalpy upon mutation of Arg¹⁰⁶ → Ala, consistent with the loss of attractive electrostatic interactions, there was a significant compensatory increase in binding entropy due to a rearrangement of hydrophobic interactions.²⁵ This was confirmed by a crystal structure of oleic acid binding to a rI-FABP Arg¹⁰⁶ → Gln mutant, where the binding orientation of the C-5 to C-18 portion of oleic acid hydrocarbon chain was shown to have a similar orientation to oleic acid bound to wild-type FABP, whereas the C-1 to C-4 section of the oleic acid tail displayed greater disorder when bound to the mutant in comparison to wild type, presumably in response to the reduced charge–charge interactions.²⁷ Similar findings have been reported in other systems where structurally related ligands bind to their target proteins with similar affinities but the enthalpic and entropic contributions to their binding affinities are quite different, suggesting differences in the mechanism of binding.²⁸ The entropic compensation for the loss of ionic interaction previously observed for FA binding to mutants of I-FABP may provide an explanation for the equal or higher binding affinity of the noncarboxylate fibrates esters for L-FABP in the current studies. Thus the CSP and modeling data for fenofibric acid (and the other carboxylate-containing molecules) are consistent with the presence of an ionic interaction with Arg¹²² of L-FABP, and this is supported by predominantly enthalpic binding. Such an interaction is not possible with the ester fenofibrate (or with clofibrate), but in this case a different mode of binding is observed. Thus the enthalpic contribution to binding is reduced (presumably due to loss of the ionic interaction), but this is more than compensated for by a more favorable entropy, such that fenofibrate

binds with higher affinity than fenofibric acid. This notion is supported by the CSP and modeling data which show that the esters, fenofibrate and clofibrate, occupy a slightly different location to the carboxylate-containing fibrates while maintaining a similar general mode of binding.

Hypolipidemic drugs such as bezafibrate and fenofibrate target the nuclear receptor PPAR α to initiate expression of lipid metabolism enzymes.^{17,29} Clofibrate is known to increase L-FABP expression in hepatocytes,³⁰ and examination of the role of L-FABP in bezafibrate transport within hepatocytes suggests a positive correlation between PPAR α activation and intracellular L-FABP concentrations.¹⁷ Previous studies have also shown that L-FABP interacts directly with PPAR α and PPAR γ and have hypothesized that L-FABP has a role as a “cytosolic receptor” for lipids and lipid lowering drugs, shuttling the ligands to the nucleus for PPAR activation.^{17,31} L-FABP therefore plays a role in the uptake and cellular disposition of fatty acids, and the current studies are indicative of a potential role in the cellular disposition of a much broader range of ligands. In the current study, we have provided a structural rationale for the observation that ligands that do not contain a terminal carboxylate are capable of binding to L-FABP with high affinity and suggest that this may reflect an enthalpy–entropy compensation effect. Enthalpy–entropy compensation arises due to a correlation between then enthalpy of binding and translational and rotational entropy of binding.^{32,33} Thus, more exothermic reactions are correlated with a greater translational and rotational entropic cost of binding. The greater entropic cost is often related to the residual mobility of the ligand in the complex.^{32,33} Although these general principles are established and have been demonstrated in a range of systems,^{28,34,35} the mechanistic basis of enthalpy–entropy compensation and its role in protein–ligand interactions remains poorly understood.³⁶ Notwithstanding, the current data indicates the potential of high affinity binding to L-FABP for a much broader range of ligands as a terminal carboxylate is not absolutely required. Indeed, the current data suggests that substitution of the terminal carboxylate with a hydrophobic moiety enhances overall binding affinity because the beneficial contribution to the free energy of binding of the interaction of the hydrophobic tail is greater than the enthalpically favorable electrostatic interaction of the terminal carboxylate with Arg¹²² in the carboxylate binding site. The consequence of binding to rL-FABP on the cellular disposition of lipophilic drugs is subject to ongoing investigations.

Experimental Procedures

Materials. Compounds used in this study are shown in Table 1 and were obtained from Sigma-Aldrich (Sydney, NSW, Australia). Purity was determined by elemental analysis, which revealed that all test compounds were $\geq 95\%$ pure. Isopropyl β -D-thiogalactopyranoside was purchased from Merck (Victoria, Australia). *Escherichia coli* strain BL21 Codon Plus (DE3)-RIL was purchased from Stratagene (La Jolla, CA). All other reagents were of the highest purity available commercially.

Expression and Purification of Rat L-FABP. Recombinant rL-FABP was expressed in BL21(DE3)/pTrc99A host/vector expression system using minor modifications of our previously described procedure.³⁷ The pTrc99-rL-FABP expression plasmid is available from the Addgene Plasmid Repository (<http://addgene.org>) under the plasmid identification code 13577. Briefly, the cells were grown in ¹⁵N–¹³C-labeled minimal media³⁸ containing ampicillin (100 μ g/mL) before induction with

1 mM IPTG. Cells were harvested by centrifugation (4000g for 30 min at 4 °C) 4 h post induction. The pellets were resuspended in buffer A (50 mM Tris-HCl, pH 8.0, 150 mM NaCl, 1 mM DTT, 0.5 mM EDTA) and lysed by sonication. The resulting homogenate was clarified by centrifugation (12000g for 30 min at 4 °C). Ammonium sulfate was added to the supernatant to 60% saturation, and the soluble fraction was recovered by centrifugation (20000g for 20 min at 4 °C). The soluble fraction was resolved by application to a Phenyl Sepharose HP 16/10 column (GE Health Care, Sydney, NSW, Australia). rL-FABP was eluted with a linear gradient from 100 to 0% 1.0 M (NH₄)₂SO₄ over 1 column volume and fractions containing L-FABP identified by SDS-PAGE. Nucleic acids were removed by centrifugation (20000g for 30 min) following addition of protamine sulfate (0.1% w/v). Protein solution was buffer exchanged into buffer A and applied to a MonoQ HR 10/10 column (GE Health Care, Sydney, NSW, Australia) in the same buffer. rL-FABP was eluted in the unbound fraction. rL-FABP containing fractions were exchanged into buffer B (50 mM Tris-HCl, pH 8.0, 1.0 M (NH₄)₂SO₄, 1 mM DTT, 0.5 mM EDTA) and applied to a Phenyl Sepharose HP 16/10 column as a final polishing step and eluted as described above. Fractions containing rL-FABP were pooled and buffer exchanged into NMR buffer (20 mM MES pH 5.5, 150 mM NaCl, 1.0 mM DTT, 0.5 mM EDTA, 10% D₂O) and concentrated by ultrafiltration. Homogeneity of the purified protein was assessed by SDS-PAGE (silver staining) and by electrospray ionization mass spectrometry on a Micromass Platform II liquid chromatography/quadrupole mass spectrometry system (Manchester, UK). Protein concentration was determined by UV-visible spectrophotometry using a molar extinction coefficient at 280 nm of 6400 (cm M)⁻¹.

NMR Spectroscopy. NMR experiments were carried out on Varian Unity 600 MHz spectrometer equipped with a single axis gradient triple resonance cryoprobe. Standard triple-resonance experiments were employed to obtain assignments for rL-FABP. Data were processed using NMRPipe³⁹ and were analyzed using the program SPARKY.⁴⁰ Titrations were performed by adding microliter amounts of each test compound to a final concentration of 3 mol equiv to ¹⁵N-¹³C labeled rL-FABP (300 μM). The physicochemical properties of the ligands, as well as *K_i* values obtained in previous studies¹³ are listed in Table 1. The predicted percentage of binding at each binding site employing these *K_i* values is reported in Supporting Information Table 3. The sample was mixed and allowed to equilibrate prior to data collection. Test compounds were prepared in DMSO. Titration of up to 10% (v/v) DMSO into the protein produced no significant chemical shift perturbations.

Overall weighted average chemical shift changes (Δavg) were calculated for all residues using the equation:⁴¹

$$\Delta_{\text{avg}} = ((\delta C_{\alpha})^2 + (\delta C_{\beta})^2)^{0.5} \quad (1)$$

where δC_α and δC_β denote the changes in chemical shift between apo and holo proteins for C_α and C_β resonances, respectively. Residues which underwent the greatest changes in chemical shift were mapped onto the crystal structure of L-FABP (1LFO).¹² Significant changes were defined as more than one standard deviation greater than the mean change.

Molecular Docking. Docking calculations were performed using Glide V4.0⁴² as implemented by Maestro V7.5 (Schrodinger LLC, New York). The crystal structure of oleic acid bound-L-FABP (1LFO) and ligands used for docking were prepared following the recommended protocol within Glide. Bound oleic acids and structured water molecules were ignored during docking in the high affinity binding site; however, the oleic acid in the high affinity site of the crystal structure was retained for docking into the low affinity binding site as ligands docked into the first binding site occupied similar orientations to the oleic acid. The center of the docking grid was defined by the center of the bound

ligands as described in the original PDB entry, and the volume of the grid was set to 10 Å³. No further modifications were applied to the default settings (no scaling factor for the vdW radii of nonpolar protein atoms, 0.8 scaling for nonpolar ligand atoms). The GlideScore scoring function was used to select up to 30 poses for each ligand.

Poses obtained from Glide were grouped into clusters of poses within 2 Å of each other using a simple cluster subroutine. A representative structure from each cluster was output to pdb format. Schematic diagrams of protein–ligand interactions were produced using Ligplot.⁴³

Fluorimetric Binding Affinity Measurements and the Determination of van't Hoff Enthalpies. Fibrates binding affinity was measured fluorimetrically by monitoring the displacement of the fluorescent binding cavity probe 1-anilino-8-naphthalene sulfonic acid (ANS) as previously described.¹³ Briefly, fluorimetric measurements were performed under steady-state conditions on a Cary Eclipse fluorescence spectrophotometer (Varian, Mulgrave, Victoria, Australia) in 20 mM MES pH 5.5, 50 mM NaCl, 1.0 mM DTT, 0.5 mM EDTA buffer. Fibrates were dissolved in DMSO and titrated directly into the protein solution. The decrease in ANS fluorescence upon addition of competing ligand was monitored and plotted as a function of the concentration of free ligand. The data were fitted by nonlinear regression to a two-site competition model from which EC₅₀ values were derived and used to calculate the inhibition constant (*K_i*) for ligand binding to each site.¹³

Enthalpies for the binding of fenofibric acid, fenofibrate and clofibrate were determined by measuring *K_i* values for each drug at several different temperatures (Supporting Information Table 3) and van't Hoff plots (eq 2) of ln(*K_i*) versus 1/*T* (which is a straight line if the heat capacity is independent of temperature), from which Δ*H*^o is determined from the slope. The Gibbs free energy change (Δ*G*^o) for each drug-L-FABP binding reaction was calculated from the equilibrium dissociation constant at 25 °C as Δ*G*^o = -*RT*ln(*K_i*) and entropies (Δ*S*^o) were determined from Δ*G*^o - Δ*H*^o.

The nonintegrated linear form (*y* = *a* + *bx*) of the van't Hoff equation:

$$\ln(K_d) = (\Delta H^o/RT) - \Delta S^o/R \quad (2)$$

A plot of *y* = ln(*K_d*) versus *x* = 1/*T* yields a straight line with a slope *b* = Δ*H*^o/*R* and a *y*-intercept, *a* = -Δ*S*^o/*R*, where *R* is the universal gas constant, 1.987 cal/(mol K).

Acknowledgment. S.C. gratefully acknowledges financial support provided by an Australian Postgraduate Scholarship. T.V. is the recipient of a Peter Doherty Fellowship (384300) from the National Health and Medical Research Council, Australia. This work was supported by grants from the Australian Research Council (DP0342458, DP0664069).

Supporting Information Available: FABP sequence alignments, binding site occupancy, temperature dependence of binding affinities, ¹H-¹⁵N HSQC data for rL-FABP, docking of fenofibric acid methyl ester, and docking clusters for fenofibrate. This material is available free of charge via the Internet at <http://pubs.acs.org>.

References

- (1) Haunerland, N. H.; Spener, F. Fatty acid-binding proteins—insights from genetic manipulations. *Prog. Lipid Res.* **2004**, *43* (4), 328–349.
- (2) Chmurzynska, A. The multigene family of fatty acid-binding proteins (FABPs): function, structure, and polymorphism. *J. Appl. Genet.* **2006**, *47* (1), 39–48.
- (3) Coe, N. R.; Bernlohr, D. A. Physiological properties and functions of intracellular fatty acid-binding proteins. *Biochim. Biophys. Acta* **1998**, *1391* (3), 287–306.

- (4) Glatz, J. F.; van der Vusse, G. J. Cellular fatty acid-binding proteins: their function and physiological significance. *Prog. Lipid Res.* **1996**, *35* (3), 243–282.
- (5) Hertzfel, A. V.; Bernlohr, D. A. The mammalian fatty acid-binding protein multigene family: molecular and genetic insights into function. *Trends Endocrinol. Metab.* **2000**, *11* (5), 175–180.
- (6) Bass, N. M.; Manning, J. A. Tissue expression of three structurally different fatty acid binding proteins from rat heart muscle, liver, and intestine. *Biochem. Biophys. Res. Commun.* **1986**, *137* (3), 929–935.
- (7) Paulussen, R. J.; van Moerkerk, H. T.; Veerkamp, J. H. Immunoluminescent quantitation of fatty acid-binding proteins. Tissue distribution of liver and heart FABP types in human and porcine tissues. *Int. J. Biochem.* **1990**, *22* (4), 393–398.
- (8) Jenkins, A. E.; Hockenberry, J. A.; Nguyen, T.; Bernlohr, D. A. Testing of the portal hypothesis: analysis of a V32G, F57G, K58G mutant of the fatty acid binding protein of the murine adipocyte. *Biochemistry* **2002**, *41* (6), 2022–2027.
- (9) Veerkamp, J. H.; Maatman, R. G. Cytoplasmic fatty acid-binding proteins: their structure and genes. *Prog. Lipid Res.* **1995**, *34* (1), 17–52.
- (10) Lowe, J. B.; Boguski, M. S.; Sweetser, D. A.; Elshourbagy, N. A.; Taylor, J. M.; Gordon, J. I. Human liver fatty acid binding protein. Isolation of a full length cDNA and comparative sequence analyses of orthologous and paralogous proteins. *J. Biol. Chem.* **1985**, *260* (6), 3413–3417.
- (11) Thompson, J.; Ory, J.; Reese-Wagoner, A.; Banaszak, L. The liver fatty acid binding protein—comparison of cavity properties of intracellular lipid-binding proteins. *Mol. Cell. Biochem.* **1999**, *192* (1–2), 9–16.
- (12) Thompson, J.; Winter, N.; Terwey, D.; Bratt, J.; Banaszak, L. The crystal structure of the liver fatty acid-binding protein. A complex with two bound oleates. *J. Biol. Chem.* **1997**, *272* (11), 7140–7150.
- (13) Chuang, S.; Velkov, T.; Horne, J.; Porter, C. J.; Scanlon, M. J. Characterization of the drug binding specificity of rat liver fatty acid binding protein. *J. Med. Chem.* **2008**, *51* (13), 3755–3764.
- (14) Miller, K. R.; Cistola, D. P. Titration calorimetry as a binding assay for lipid-binding proteins. *Mol. Cell. Biochem.* **1993**, *123* (1–2), 29–37.
- (15) Richieri, G. V.; Ogata, R. T.; Kleinfeld, A. M. Equilibrium constants for the binding of fatty acids with fatty acid-binding proteins from adipocyte, intestine, heart, and liver measured with the fluorescent probe ADIFAB. *J. Biol. Chem.* **1994**, *269* (39), 23918–23930.
- (16) Wolfrum, C.; Borchers, T.; Sacchettini, J. C.; Spener, F. Binding of fatty acids and peroxisome proliferators to orthologous fatty acid binding proteins from human, murine, and bovine liver. *Biochemistry* **2000**, *39* (6), 1469–1474.
- (17) Wolfrum, C.; Borrmann, C. M.; Borchers, T.; Spener, F. Fatty acids and hypolipidemic drugs regulate peroxisome proliferator-activated receptors alpha- and gamma-mediated gene expression via liver fatty acid binding protein: a signaling path to the nucleus. *Proc. Natl. Acad. Sci. U.S.A.* **2001**, *98* (5), 2323–2328.
- (18) Velkov, T.; Chuang, S.; Wielens, J.; Sakellaris, H.; Charman, W. N.; Porter, C. J.; Scanlon, M. J. The interaction of lipophilic drugs with intestinal fatty acid-binding protein. *J. Biol. Chem.* **2005**, *280* (18), 17769–17776.
- (19) Velkov, T.; Horne, J.; Laguerre, A.; Jones, E.; Scanlon, M. J.; Porter, C. J. Examination of the role of intestinal Fatty Acid-binding protein in drug absorption using a parallel artificial membrane permeability assay. *Chem. Biol.* **2007**, *14* (4), 453–465.
- (20) He, Y.; Yang, X.; Wang, H.; Estephan, R.; Francis, F.; Kodukula, S.; Storch, J.; Stark, R. E. Solution-state molecular structure of apo and oleate-liganded liver fatty acid-binding protein. *Biochemistry* **2007**, *46* (44), 12543–12556.
- (21) Richieri, G. V.; Ogata, R. T.; Kleinfeld, A. M. Thermodynamic and kinetic properties of fatty acid interactions with rat liver fatty acid-binding protein. *J. Biol. Chem.* **1996**, *271* (49), 31068–31074.
- (22) Hagan, R. M.; Davies, J. K.; Wilton, D. C. The effect of charge reversal mutations in the alpha-helical region of liver fatty acid binding protein on the binding of fatty-acyl CoAs, lysophospholipids and bile acids. *Mol. Cell. Biochem.* **2002**, *239* (1–2), 55–60.
- (23) Thumser, A. E.; Evans, C.; Worrall, A. F.; Wilton, D. C. Effect on ligand binding of arginine mutations in recombinant rat liver fatty acid-binding protein. *Biochem. J.* **1994**, *297* (Pt 1), 103–107.
- (24) Thumser, A. E.; Voysey, J.; Wilton, D. C. Mutations of recombinant rat liver fatty acid-binding protein at residues 102 and 122 alter its structural integrity and affinity for physiological ligands. *Biochem. J.* **1996**, *314* (Pt 3), 943–949.
- (25) Richieri, G. V.; Low, P. J.; Ogata, R. T.; Kleinfeld, A. M. Mutants of rat intestinal fatty acid-binding protein illustrate the critical role played by enthalpy–entropy compensation in ligand binding. *J. Biol. Chem.* **1997**, *272* (27), 16737–16740.
- (26) Sacchettini, J. C.; Gordon, J. I.; Banaszak, L. J. Crystal structure of rat intestinal fatty acid-binding protein. Refinement and analysis of the *Escherichia coli*-derived protein with bound palmitate. *J. Mol. Biol.* **1989**, *208* (2), 327–339.
- (27) Eads, J.; Sacchettini, J. C.; Kromminga, A.; Gordon, J. I. *Escherichia coli*-derived rat intestinal fatty acid binding protein with bound myristate at 1.5 Å resolution and I-FABPArg106→Gln with bound oleate at 1.74 Å resolution. *J. Biol. Chem.* **1993**, *268* (35), 26375–26385.
- (28) Gerlach, C.; Smolinski, M.; Steuber, H.; Sotriffer, C. A.; Heine, A.; Hangauer, D. G.; Klebe, G. Thermodynamic inhibition profile of a cyclopentyl and a cyclohexyl derivative towards thrombin: the same but for different reasons. *Angew. Chem., Int. Ed.* **2007**, *46* (44), 8511–8514.
- (29) Brouillette, C.; Bosse, Y.; Perusse, L.; Gaudet, D.; Vohl, M. C. Effect of liver fatty acid binding protein (FABP) T94A missense mutation on plasma lipoprotein responsiveness to treatment with fenofibrate. *J. Hum. Genet.* **2004**, *49* (8), 424–432.
- (30) Rajaraman, G.; Burczynski, F. J. Effect of dexamethasone, 2-bromopalmitate and clofibrate on L-FABP mediated hepatoma proliferation. *J. Pharm. Pharmacol.* **2004**, *56* (9), 1155–1161.
- (31) Schroeder, F.; Petrescu, A. D.; Huang, H.; Atshaves, B. P.; McIntosh, A. L.; Martin, G. G.; Hostetler, H. A.; Vespa, A.; Landrock, D.; Landrock, K. K.; Payne, H. R.; Kier, A. B. Role of fatty acid binding proteins and long chain fatty acids in modulating nuclear receptors and gene transcription. *Lipids* **2008**, *43* (1), 1–17.
- (32) Calderone, C. T.; Williams, D. H. An enthalpic component in cooperativity: the relationship between enthalpy, entropy, and noncovalent structure in weak associations. *J. Am. Chem. Soc.* **2001**, *123* (26), 6262–6267.
- (33) Williams, D. H.; Stephens, E.; O'Brien, D. P.; Zhou, M. Understanding noncovalent interactions: ligand binding energy and catalytic efficiency from ligand-induced reductions in motion within receptors and enzymes. *Angew. Chem., Int. Ed.* **2004**, *43* (48), 6596–6616.
- (34) Bryson, J. W.; Betz, S. F.; Lu, H. S.; Suich, D. J.; Zhou, H. X.; O'Neil, K. T.; DeGrado, W. F. Protein design: a hierarchical approach. *Science* **1995**, *270* (5238), 935–941.
- (35) Day, C. L.; Smits, C.; Fan, F. C.; Lee, E. F.; Fairlie, W. D.; Hinds, M. G. Structure of the BH3 domains from the p53-inducible BH3-only proteins Noxa and Puma in complex with Mcl-1. *J. Mol. Biol.* **2008**, *380* (5), 958–971.
- (36) Krishnamurthy, V. M.; Bohall, B. R.; Semetey, V.; Whitesides, G. M. The paradoxical thermodynamic basis for the interaction of ethylene glycol, glycine, and sarcosine chains with bovine carbonic anhydrase II: an unexpected manifestation of enthalpy/entropy compensation. *J. Am. Chem. Soc.* **2006**, *128* (17), 5802–5812.
- (37) Velkov, T.; Chuang, S.; Prankerd, R.; Sakellaris, H.; Porter, C. J.; Scanlon, M. J. An improved method for the purification of rat liver-type fatty acid binding protein from *Escherichia coli*. *Protein Expression Purif.* **2005**, *44* (1), 23–31.
- (38) Marley, J.; Lu, M.; Bracken, C. A method for efficient isotopic labeling of recombinant proteins. *J. Biomol. NMR* **2001**, *20* (1), 71–75.
- (39) Delaglio, F.; Grzesiek, S.; Vuister, G. W.; Zhu, G.; Pfeifer, J.; Bax, A. NMRPipe: a multidimensional spectral processing system based on UNIX pipes. *J. Biomol. NMR* **1995**, *6* (3), 277–293.
- (40) Goddard, T. D.; Kneller, D. G. *SPARKY 3*, 2001.
- (41) Ayed, A.; Mulder, F. A.; Yi, G. S.; Lu, Y.; Kay, L. E.; Arrowsmith, C. H. Latent and active p53 are identical in conformation. *Nat. Struct. Biol.* **2001**, *8* (9), 756–760.
- (42) Friesner, R. A.; Banks, J. L.; Murphy, R. B.; Halgren, T. A.; Klicic, J. J.; Mainz, D. T.; Repasky, M. P.; Knoll, E. H.; Shelley, M.; Perry, J. K.; Shaw, D. E.; Francis, P.; Shenkin, P. S. Glide: a new approach for rapid, accurate docking and scoring. 1. Method and assessment of docking accuracy. *J. Med. Chem.* **2004**, *47* (7), 1739–1749.
- (43) Wallace, A. C.; Laskowski, R. A.; Thornton, J. M. LIGPLOT: a program to generate schematic diagrams of protein–ligand interactions. *Protein Eng.* **1995**, *8* (2), 127–134.